

Supporting Information

ZIF-67-derived $\text{Co}_3\text{O}_4@\text{carbon}$ protected by oxygen buffering CeO_2 as an efficient catalyst for boosting oxygen reduction/evolution reactions

Xuerui Li^a, Shijie You^b, Jiannan Du^a, Ying Dai^{a,c,*}, Hun Chen^a, Zhuang Cai^{a,*}, Nanqi Ren^b, Jinlong Zou^{a,*}

^a Key Laboratory of Functional Inorganic Material Chemistry, Ministry of Education of the People's Republic of China, School of Chemistry and Materials Science, Heilongjiang University, Harbin, 150080, China;

^b State Key Laboratory of Urban Water Resource and Environment, School of Environment, Harbin Institute of Technology, Harbin 150090, P. R. China;

^cSchool of Civil Engineering, Heilongjiang Institute of Technology, Harbin 150050, China.

Corresponding author (s):

*Ying Dai, Zhuang Cai, Jinlong Zou.

^aXuefu Road 74#, Nangang District, Harbin, 150080, China.

Tel.: +86-451-86608616; Fax: +86-451-86608616.

E-mail: zjh_0308@126.com (Y. Dai); hlju_chem218c@163.com (Z. Cai); zoujinlong@aliyun.com (J. L. Zou).

1. Experimental section

1.1 Material Characterizations

Herein, the structure, morphology and compositions of the as-prepared materials were characterized by X-ray diffraction (XRD), X-ray photoelectron spectroscopy (XPS), N₂ adsorption/desorption isotherms, transmission electron microscopy (TEM), scanning electron microscope (SEM) and elemental mappings (energy-dispersive X-ray spectroscopy, EDS). The collection of XRD data was performed using a Rigaku D/max 2500 diffractometer equipped with Cu-K α radiation ($k=1.5406\text{ \AA}$, 40 kV, 20mA). The Kratos-AXISUL TRA DLD X-ray photoelectron spectrometer equipped with Al K α radiation was used to record XPS data. "XPS peak" software was used to fit the XPS data of each element. N₂ adsorption and desorption isotherms were determined at 77 k using a micron-scale three-star adsorption analyzer. Brunauer-Emmett-Teller (BET) method and Barrett-Joyner-Halenda (BJH) theory were used to analyze the specific surface area and pore size distribution (PSD), respectively. TEM and high-resolution TEM (HRTEM) images were collected on a JEM-2100 electron microscope (JEOL) at an accelerated voltage of 200 kV. SEM images and elemental mappings were collected using an S-4800 (Hitachi, Japan) scanning electron microscope at an acceleration voltage of 5.0 kV. The electron paramagnetic resonance (EPR) spectra were obtained by a JES-FA200 X band spectrometer. The settings of EPR spectrometer were shown as follows: center field=3512 G, microwave frequency=9.42 GHz, and microwave power=20 mW.

1.2 Electrochemical measurements

All electrochemical tests were performed on a rotating disk electrode (RDE) controller connected to an electrochemical workstation (CHI760E, Shanghai, Chenhua). A three-electrode system was used for electrochemical tests, with a saturated calomel electrode (SCE) as the reference electrode, a platinum wire as the counter electrode, and a catalyst coated glassy carbon electrode (GCE) as the working electrode. In this study, the measured SCE potential was converted to the reversible

hydrogen electrode (RHE) potential based on $E_{\text{RHE}} = E_{\text{SCE}} + 0.0592 \text{ pH} + 0.2438$. The method for preparing the catalyst ink was shown as follows: 5 mg of the catalyst were dispersed in a mixture of 50 μL of 5 wt.% Nafion (Aldrich) and 100 μL ethanol, and then the mixture was sonicated for 30 min to form the uniform ink. The surface of GCE (4 mm in diameter) was coated with 5 μL of the prepared ink, with a catalyst coating area of 0.126 cm^2 . Commercial Pt/C (10 wt.%) and RuO₂ were used as the reference catalysts in this study.

All ORR tests were performed in 0.1 M KOH aqueous solution. Before each test, the electrolyte solution was aerated with pure O₂ for 30 min. Cyclic voltammetry (CV) tests were conducted from -1.0 to 0.2 V in electrolyte solution saturated with O₂ at a scan rate of 10 mV s⁻¹. During the CV measurement, the RDE electrode was rotated at a constant speed of 1600 rpm. Linear sweep voltammetry (LSV) test was performed in the potential range identical to that of CV at a scan rate of 5 mV s⁻¹. Electrochemical impedance spectroscopy (EIS), Chronoamperometry (CA) and Tafel tests were performed using the reported methods.¹ In addition, an important parameter for evaluating OER activity is the Tafel slope b, and the corresponding Tafel plots are constructed based on the LSV curves. Determined by the following Tafel equation:

$$\eta = a + b \log|J| \quad (1)$$

Where η is the overpotential, b is the Tafel slope, and J is the current density.

RDE tests were measured in an O₂-saturated electrolyte solution at a scan rate of 5 mV s⁻¹ and a different rotation speed of 400 to 2500 rpm. To study the ORR kinetics, the Koutecky-Levich (K-L) equation was used to determine the number of transferred electrons (n) for each O₂ molecule at different rotation rates.

$$\frac{1}{j} = \frac{1}{j_0} + \frac{1}{j_k} = \frac{1}{B\omega^{1/2}} + \frac{1}{nFkc_0} \quad (2)$$

$$B = 0.62nFC_0D_0^{2/3}\nu^{-1/6} \quad (3)$$

In Equation 2, J , J_L , and J_K corresponded to the measured current, the diffusion limit current, and the dynamic current, respectively. The values of the angular velocity ω ($2\pi \times$ rotation speed) and the Faraday constant F (96485 C mol $^{-1}$) were already known. In 0.1 M KOH electrolyte, the values of diffusion coefficient and saturation concentration of O₂ are 1.9×10^{-5} cm 2 s $^{-1}$ (D₀) and 1.2×10^{-6} mol cm $^{-3}$ (C₀), respectively. The kinematic viscosity (ν) of the electrolyte was 0.01 cm 2 s $^{-1}$, and the number of electrons "n" were obtained by calculating the slope of J^{-1} vs. $\omega^{-1/2}$ in the plot.

Rotating ring-disk electrode (RRDE) tests were conducted at a rotation speed of 1600 rpm with a scan rate of 10 mV s $^{-1}$ in O₂-saturated 0.1 M KOH solution. Hydrogen peroxide yield (H₂O₂, %) and electron transfer number (n) were calculated using the RRDE voltammograms. The used Equations (4 and 5) were shown as follows:

$$n = 4 \times \frac{I_d}{I_d + (I_r / N)} \quad (4)$$

$$\text{H}_2\text{O}_2 \% = 200 \times \frac{I_r / N}{I_d + (I_r / N)} \quad (5)$$

Where I_D and I_R corresponded to the disk current and the ring current, respectively; N represented the H₂O₂ collection efficiency of the Pt ring, and the value was 0.37.

OER tests were performed in 0.1 M KOH electrolyte solution. Linear sweep voltammetry (LSV) was carried out at a scan rate of 2 mV s $^{-1}$ for the polarization curves, without iR-compensation correction. The durability of catalyst after 1000 CV cycles was studied by using the accelerated durability test (ADT). EIS tests were performed at 1.58 V vs. RHE with frequencies ranging from 100 kHz to 100 MHz. The electrochemically active area was calculated from the electrical double layer capacitance measurements, which were cycled at scan rates of 40, 60, 80, 100, and 120 mV s $^{-1}$

with a potential range from 0.96 to 1.06 V vs. RHE. Tafel and CA tests were performed using the reported methods.^{2,3}

Moreover, one of the genuine approaches for electrochemical active sites measurement is the electrochemical surface area calculation via electrical double-layer capacitance (C_{dl}) using cyclic voltammetry (CV).⁴ Which are converted to ECSA according to the equation below.⁵

$$ECSA = C_{dl}/C_s \quad (6)$$

The specific capacitance (C_s) value $C_s=0.040 \text{ mF cm}^{-2}$ in 0.1 M KOH is adopted from previous reports.

Turnover Frequency (TOF) was calculated from the OER current density, assuming that the surface active Co and Ce atoms undergoing redox reactions before the start of the OER were only involved in the electrocatalysis of OER. We have calculated the TOF using the OER current density at the potentials from 1.58 to 1.88 V. The corresponding Equations 7 and 8 were shown as follows:

$$TOF = \frac{j \times N_A}{F \times n \times \Gamma} \quad (7)$$

$$\Gamma = \frac{A}{Scan\ rate \times e} \quad (8)$$

Where j referred to the current density, n corresponded to number of electrons, Γ was the surface concentration, A was the area of CV associated with the redox characteristics of CV, the Scan rate was 0.3 V s^{-1} , e represented the amount of electron charge and the value was $1.602 \times 10^{-19} \text{ C}$. In addition, the values of the Avogadro number N_A and the Faraday constant F were already known.³

Faraday efficiency (FE) measurements had been recognized as the important activity parameters, and FE should be determined to ensure that the provided energy was more efficiently used for water oxidation than other side reactions. The Equation 9 for calculating FE was shown as follows:^{6,7}

$$FE = \frac{I_r}{I_d \times N} \quad (9)$$

Where I_r and I_d were the ring current and the disk current, respectively; N (0.37) was the current collection efficiency of RRDE.

2. Results and discussion

Table S1. Chemical compositions of $\text{Co}_3\text{O}_4@\text{Z67-NT}@Ce\text{O}_2$ electrocatalysts obtained from XPS analyses.

Samples	C (wt. %)	N (wt. %)	O (wt. %)	Co (wt.%)	Ce (wt.%)
$\text{Co}_3\text{O}_4@\text{Z67-N500}@Ce\text{O}_2$	12.6	0.18	24.10	49.40	13.72
$\text{Co}_3\text{O}_4@\text{Z67-N600}@Ce\text{O}_2$	42.52	12.85	16.69	19.31	8.63
$\text{Co}_3\text{O}_4@\text{Z67-N700}@Ce\text{O}_2$	51.03	2.59	18.65	5.86	21.90
$\text{Co}_3\text{O}_4@\text{Z67-N800}@Ce\text{O}_2$	38.38	1.57	24.71	18.79	16.55
$\text{Co}_3\text{O}_4@\text{Z67-N900}@Ce\text{O}_2$	46.06	0.73	21.71	21.03	10.47

Table S2. Chemical compositions of C 1s peaks for $\text{Co}_3\text{O}_4@\text{Z67-NT}@{\text{CeO}_2}$ electrocatalysts obtained from XPS analyses.

Analysis of the C 1s XPS data for the $\text{Co}_3\text{O}_4@\text{Z67-NT}@{\text{CeO}_2}$ materials				
Samples	Chemical components (%) of the C 1s peaks			
	C=C	C–C	C–O	C=O
$\text{Co}_3\text{O}_4@\text{Z67-N500}@{\text{CeO}_2}$	60.23	24.63	8.49	6.65
$\text{Co}_3\text{O}_4@\text{Z67-N600}@{\text{CeO}_2}$	75.99	15.03	5.40	3.58
$\text{Co}_3\text{O}_4@\text{Z67-N700}@{\text{CeO}_2}$	58.02	22.22	11.26	8.50
$\text{Co}_3\text{O}_4@\text{Z67-N800}@{\text{CeO}_2}$	43.78	36.13	12.27	7.82
$\text{Co}_3\text{O}_4@\text{Z67-N900}@{\text{CeO}_2}$	50.98	29.41	9.81	9.80

Table S3. Chemical compositions of N 1s peaks for $\text{Co}_3\text{O}_4@\text{Z67-NT}@{\text{CeO}_2}$ electrocatalysts obtained from XPS analyses.

Analysis of the N 1s XPS data for the $\text{Co}_3\text{O}_4@\text{Z67-NT}@{\text{CeO}_2}$ materials			
Sample	Chemical components (%) of the N 1s peaks		
	pyridinic N	pyrrolic N	graphitic N
$\text{Co}_3\text{O}_4@\text{Z67-N500}@{\text{CeO}_2}$	19.32	30.17	50.51
$\text{Co}_3\text{O}_4@\text{Z67-N600}@{\text{CeO}_2}$	76.96	13.98	9.06
$\text{Co}_3\text{O}_4@\text{Z67-N700}@{\text{CeO}_2}$	37.17	36.83	26.00
$\text{Co}_3\text{O}_4@\text{Z67-N800}@{\text{CeO}_2}$	42.77	39.09	18.14
$\text{Co}_3\text{O}_4@\text{Z67-N900}@{\text{CeO}_2}$	11.58	67.49	20.93

Table S4. Chemical compositions of O 1s peaks for $\text{Co}_3\text{O}_4@\text{Z67-NT}@{\text{CeO}_2}$ electrocatalysts obtained from XPS analyses.

Analysis of the O 1s XPS data for the $\text{Co}_3\text{O}_4@\text{Z67-NT}@{\text{CeO}_2}$ materials			
Sample	Chemical components (%) of the O 1s peaks		
	O α	O β	O γ
$\text{Co}_3\text{O}_4@\text{Z67-N500}@{\text{CeO}_2}$	45.27	29.07	25.66
$\text{Co}_3\text{O}_4@\text{Z67-N600}@{\text{CeO}_2}$	44.51	31.42	24.07
$\text{Co}_3\text{O}_4@\text{Z67-N700}@{\text{CeO}_2}$	47.98	34.17	17.85
$\text{Co}_3\text{O}_4@\text{Z67-N800}@{\text{CeO}_2}$	64.08	21.83	14.08
$\text{Co}_3\text{O}_4@\text{Z67-N900}@{\text{CeO}_2}$	9.07	25.19	65.74

Table S5. Chemical compositions of Co 2p peaks for $\text{Co}_3\text{O}_4@\text{Z67-NT}@{\text{CeO}_2}$ electrocatalysts obtained from XPS analyses.

Analysis of the Co 2p XPS data for the $\text{Co}_3\text{O}_4@\text{Z67-NT}@{\text{CeO}_2}$ materials		
Sample	Chemical components (%) of the Co 2p peaks	
	Co^{2+}	Co^{3+}
$\text{Co}_3\text{O}_4@\text{Z67-N500}@{\text{CeO}_2}$	57.97	42.03
$\text{Co}_3\text{O}_4@\text{Z67-N600}@{\text{CeO}_2}$	60.87	39.13
$\text{Co}_3\text{O}_4@\text{Z67-N700}@{\text{CeO}_2}$	62.98	37.02
$\text{Co}_3\text{O}_4@\text{Z67-N800}@{\text{CeO}_2}$	60.39	39.61
$\text{Co}_3\text{O}_4@\text{Z67-N900}@{\text{CeO}_2}$	59.33	40.67

Table S6. Chemical compositions of Ce 3d peaks for $\text{Co}_3\text{O}_4@\text{Z67-NT}@{\text{CeO}_2}$ electrocatalysts obtained from XPS analyses.

Analysis of the Ce 3d XPS data for the $\text{Co}_3\text{O}_4@\text{Z67-NT}@{\text{CeO}_2}$ materials		
Sample	Chemical components (%) of the Ce 3d peaks	
	Ce ³⁺ (U ₂ + V ₂)	Ce ⁴⁺ (U ₁ + U ₃ +U ₄ +V ₁ +V ₃ +V ₄)
$\text{Co}_3\text{O}_4@\text{Z67-N500}@{\text{CeO}_2}$	23.96	76.04
$\text{Co}_3\text{O}_4@\text{Z67-N600}@{\text{CeO}_2}$	31.09	68.91
$\text{Co}_3\text{O}_4@\text{Z67-N700}@{\text{CeO}_2}$	36.91	63.09
$\text{Co}_3\text{O}_4@\text{Z67-N800}@{\text{CeO}_2}$	34.32	65.68
$\text{Co}_3\text{O}_4@\text{Z67-N900}@{\text{CeO}_2}$	33.50	66.50

Table S7. Textural properties of the $\text{Co}_3\text{O}_4@\text{Z67-N700}$ and $\text{Co}_3\text{O}_4@\text{Z67-NT}@{\text{CeO}_2}$ composites.

Samples	S_{BET}	Pore volume ($\text{cm}^3 \text{ g}^{-1}$)	Average pore width (nm)
$\text{Co}_3\text{O}_4@\text{Z67-N700}$	350.64	0.11	5.29
$\text{Co}_3\text{O}_4@\text{Z67-N500}@{\text{CeO}_2}$	141.81	0.10	9.39
$\text{Co}_3\text{O}_4@\text{Z67-N600}@{\text{CeO}_2}$	188.04	0.10	11.02
$\text{Co}_3\text{O}_4@\text{Z67-N700}@{\text{CeO}_2}$	267.27	0.09	6.21
$\text{Co}_3\text{O}_4@\text{Z67-N800}@{\text{CeO}_2}$	242.49	0.17	6.97
$\text{Co}_3\text{O}_4@\text{Z67-N900}@{\text{CeO}_2}$	220.51	0.15	12.31

Table S8. Summary of the ORR electrocatalytic activity of various catalysts in alkaline electrolyte.

Catalysts	E ₀ (Vvs. RHE)	E _{1/2} (V vs. RHE)	J _L (mA cm ⁻²)	References
Co ₃ O ₄ @Z67-N700@CeO ₂	0.94	0.88	6.75	This work
CeO ₂ /MnO ₂	0.92	0.75	4.97	8
(Co@NPC-900) ₁₂	1.05	0.824	5.26	9
Co@Co ₃ O ₄ @C-CM	0.93	0.81	-	10
Co ₃ O ₄ -CeO ₂ /KB	-	0.83	5.35	11
Co ₉ S ₈ /NPCP@rGO	0.89	0.81	5.4	12
MnO _x -CeO ₂ /KB	0.94	0.81	-	13
Co@O-NPC-700	-	0.80	5.3	14
Co/N-CNTs	0.96	0.82	5.82	15
Co ₃ O ₄ /N-rmGO	0.96	0.83	5.00	16

Table S9. Summary of the OER electrocatalytic activity of various catalysts in alkaline electrolyte.

Catalysts	$E_{j=10}$ (V vs. RHE)	References
$\text{Co}_3\text{O}_4@\text{Z}67-\text{N}700@\text{CeO}_2$	1.58	This work
700-CoO _x -C	1.59	17
$\text{Co}_3\text{O}_4@\text{Ni}$	1.64	18
ZIF-Co _{0.85} Se	1.59	19
$\text{Mn}_3\text{O}_4/\text{CoSe}_2$	1.68	20
N/Co-doped PCP	1.75	21
$\text{Co}_3\text{O}_4/\text{rGO-W}$	1.61	22
$\text{CeO}_2@\text{PIZA-1-400}$	1.60	23
ZIF-67-CNT-300	1.58	24
$\text{Co(OH)}_2@\text{RGONF}$	1.65	25

Table S10. Summary of ORR/OER activities of as-prepared catalysts in 0.1 M KOH electrolyte.

Catalysts	ORR				OER		Overall evaluation	
	E_0	$E_{1/2}$	J_L	Tafel Slope	$E_{j=10}$	Overpotential	Tafel Slope	ΔE (V vs RHE)
	(V vs RHE)	(V vs RHE)	(mA cm ⁻²)	(mV dec ⁻¹)	(V vs RHE)	(mV)	(mV dec ⁻¹)	
Co ₃ O ₄ @Z67-N700	0.93	0.86	5.14	107.9	1.72	490	103.7	0.86
Co ₃ O ₄ @Z67-N500@CeO ₂	0.81	0.65	2.83	-	1.92	690	-	1.27
Co ₃ O ₄ @Z67-N600@CeO ₂	0.91	0.84	4.16	-	1.82	590	-	0.98
Co ₃ O ₄ @Z67-N700@CeO ₂	0.94	0.88	6.75	66.8	1.58	350	80.7	0.70
Co ₃ O ₄ @Z67-N800@CeO ₂	0.95	0.88	5.15	-	1.67	440	-	0.79
Co ₃ O ₄ @Z67-N900@CeO ₂	0.89	0.82	5.04	-	1.72	490	-	0.90
Pt/C	0.95	0.87	6.75	111.0	-	-	-	-
RuO ₂	-	-	-	-	1.66	430	151.6	0.79

Table S11. Summary of the bifunctional ORR/OER electrocatalytic activities of various catalysts in alkaline electrolyte.

Catalysts	E ₀ (V vs RHE)	E _{1/2} (V vs RHE)	J _L (mA cm ⁻²)	E _{j=10} (V vs RHE)	Overpotential (mV)	ΔE (V vs RHE)	References
Co ₃ O ₄ @Z67-N700@CeO ₂	0.94	0.88	6.75	1.58	350	0.70	This work
Co@CoO@Co ₃ O ₄ -N/C	0.85	0.75	4.90	1.67	440	0.92	26
PdCo-300	0.91	0.83	5.07	1.58	350	0.75	27
Co@Co ₃ O ₄ @/NC-900	-	0.80	4.72	1.6	370	0.80	28
Co-CeO ₂ /N-CNR	-	0.80	-	1.64	410	0.84	29
CoNC-CNF-1000	-	0.80	5.90	1.68	450	0.88	30
Co-N/PC@CNT-700	0.92	0.79	-	1.63	400	0.84	31
P-Co-NC-4	0.90	0.85	-	1.59	360	0.74	32
Co@Co ₃ O ₄ @/NC-1	-	0.84	-	1.65	420	0.81	33
Co/N-Pg	-	0.82	5.40	1.63	400	0.81	34
15%PANI/ZIF-67	0.85	0.75	4.60	1.56	330	0.81	35
Co ₁ Ni ₁ @N-C	0.91	0.82	5.3	1.73	500	0.91	36

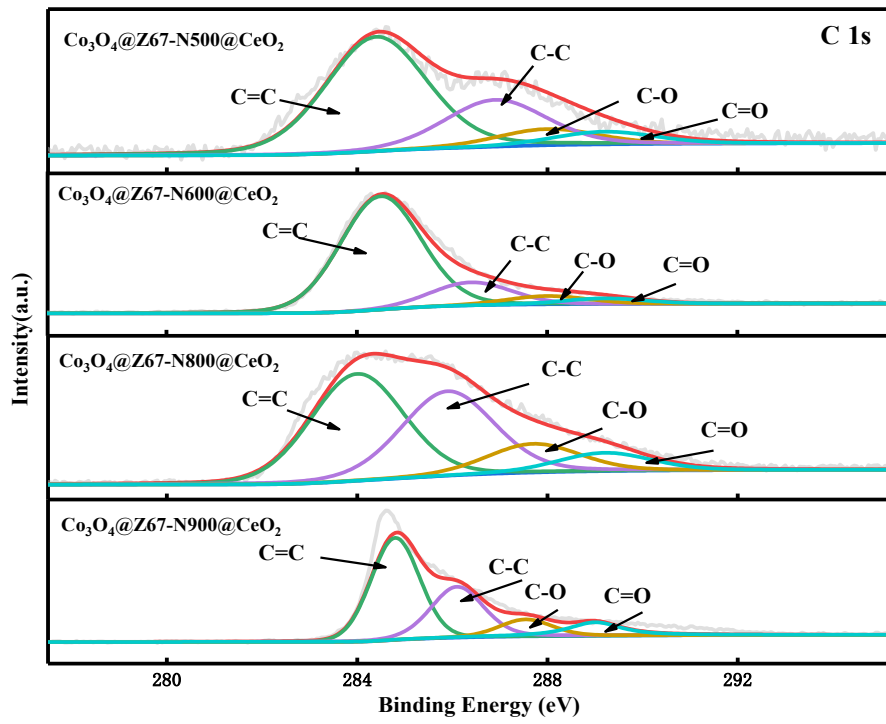


Fig. S1. High-resolution XPS spectra of C 1s for $\text{Co}_3\text{O}_4@\text{Z67-NT}@{\text{CeO}_2}$ ($T=500, 600, 800$, and 900).

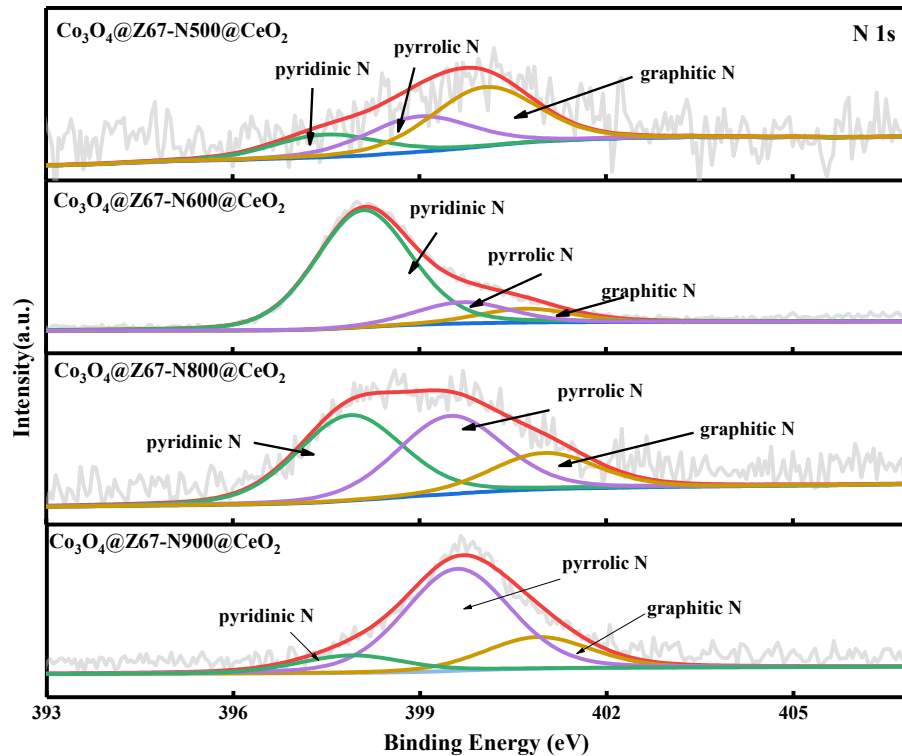


Fig. S2. High-resolution XPS spectra of N 1s for $\text{Co}_3\text{O}_4@\text{Z67-NT}@{\text{CeO}_2}$ ($T=500, 600, 800$, and 900).

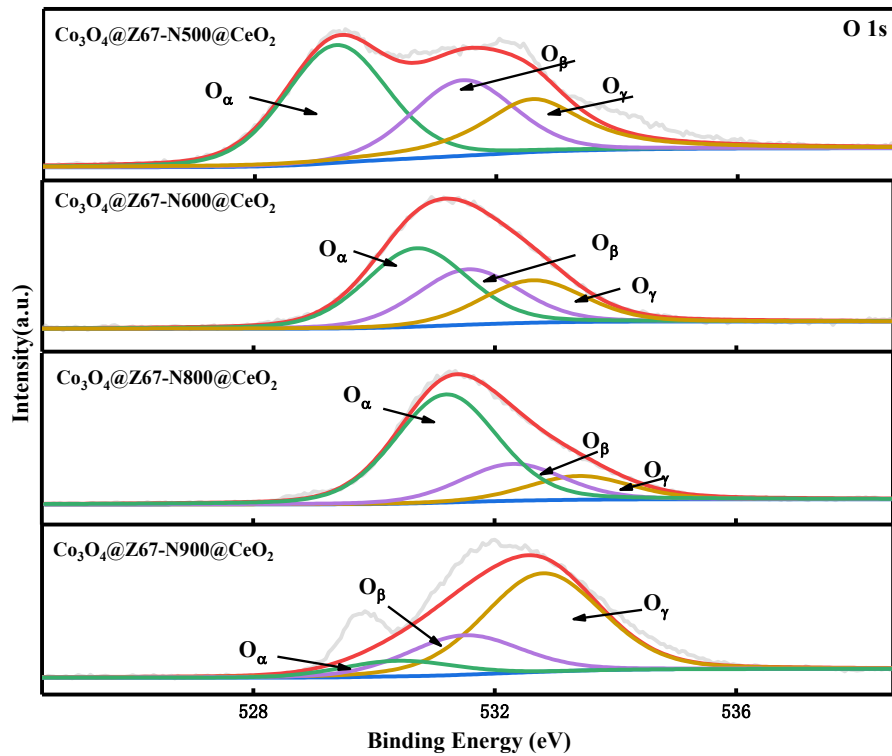


Fig. S3. High-resolution XPS spectra of O 1s for $\text{Co}_3\text{O}_4@\text{Z67-NT}@{\text{CeO}}_2$ ($T=500, 600, 800$, and 900).

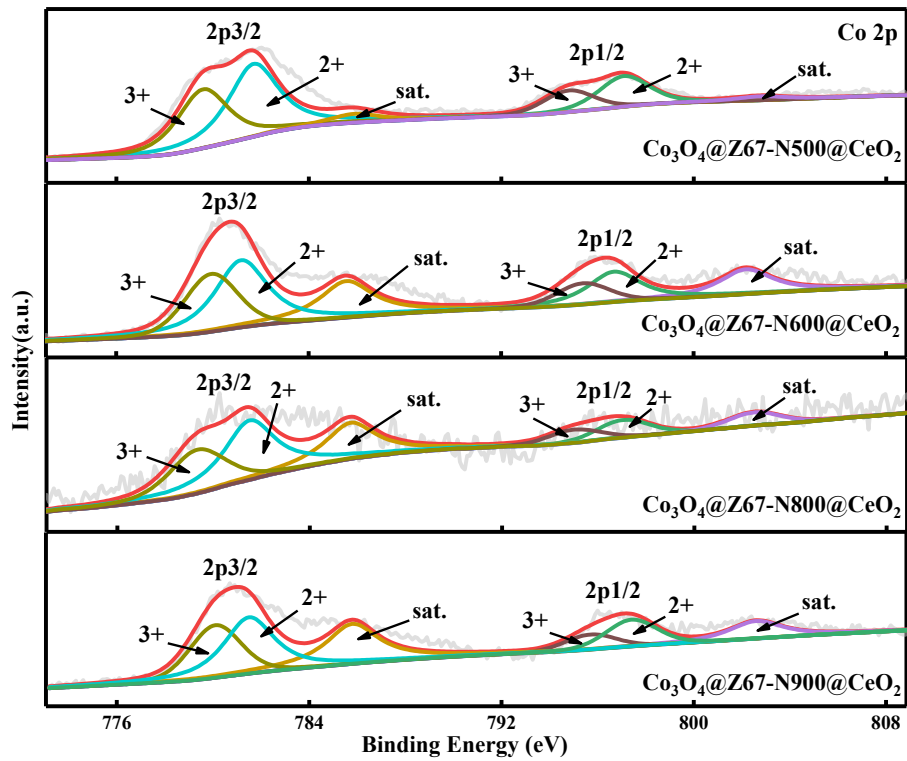


Fig. S4. High-resolution XPS spectra of Co 2p for $\text{Co}_3\text{O}_4@\text{Z67-NT}@{\text{CeO}}_2$ ($T=500, 600, 800$, and 900).

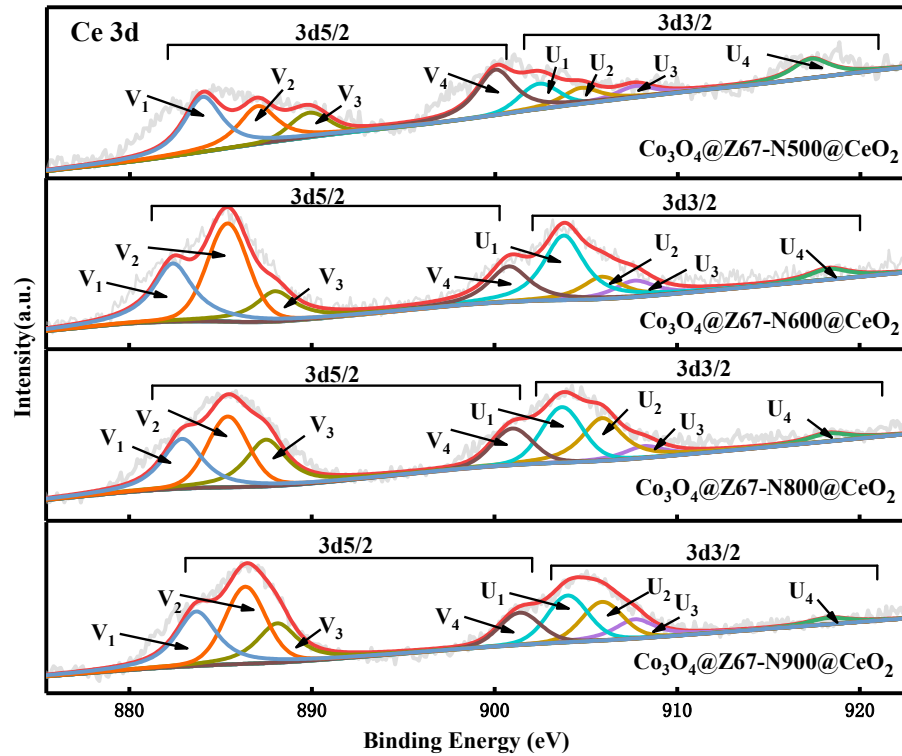


Fig. S5. High-resolution XPS spectra of Ce 3d for $\text{Co}_3\text{O}_4@\text{Z67-NT}@{\text{CeO}}_2$ ($T=500, 600, 800$, and 900).

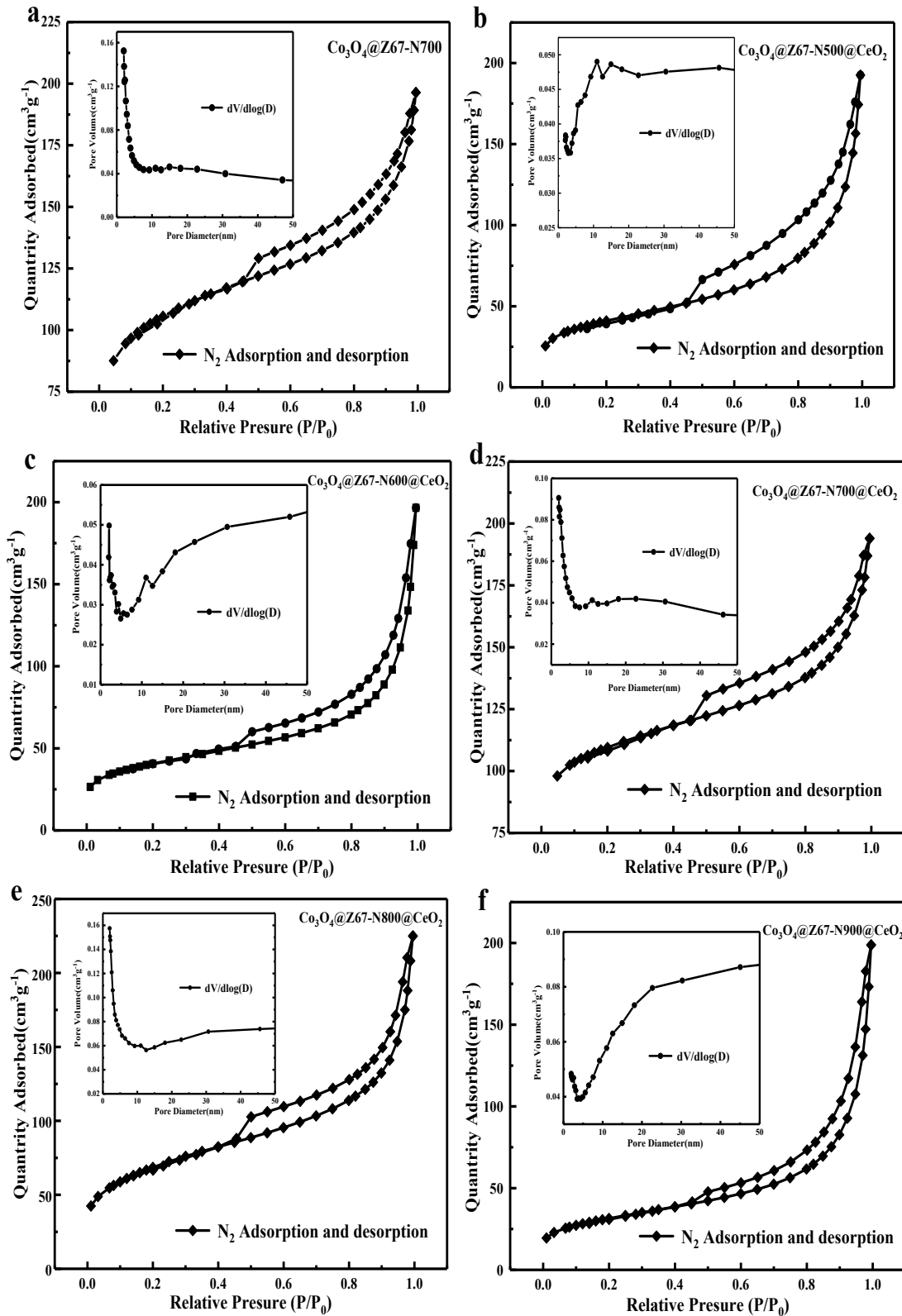


Fig. S6. N_2 adsorption/desorption isotherms and pore size distributions (inset) for the $\text{Co}_3\text{O}_4@\text{Z67-N}700$ (a) and the $\text{Co}_3\text{O}_4@\text{Z67-NT}@{\text{CeO}_2}$ [T=500(b), 600(c), 700(d), 800(e), and 900(f)]

composites.

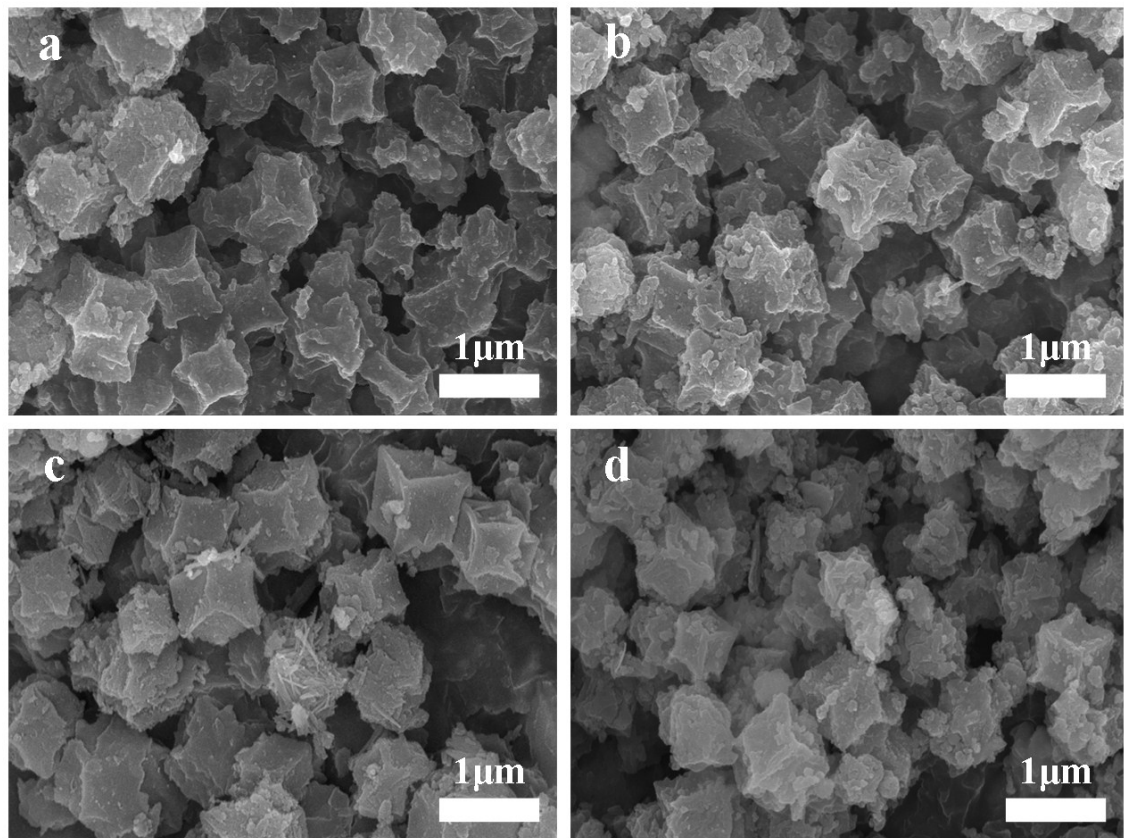


Fig. S7. SEM images of $\text{Co}_3\text{O}_4@\text{Z67-NT}@ \text{CeO}_2$ [$T=500$ (a), 600(b), 800(c), and 900(d)].

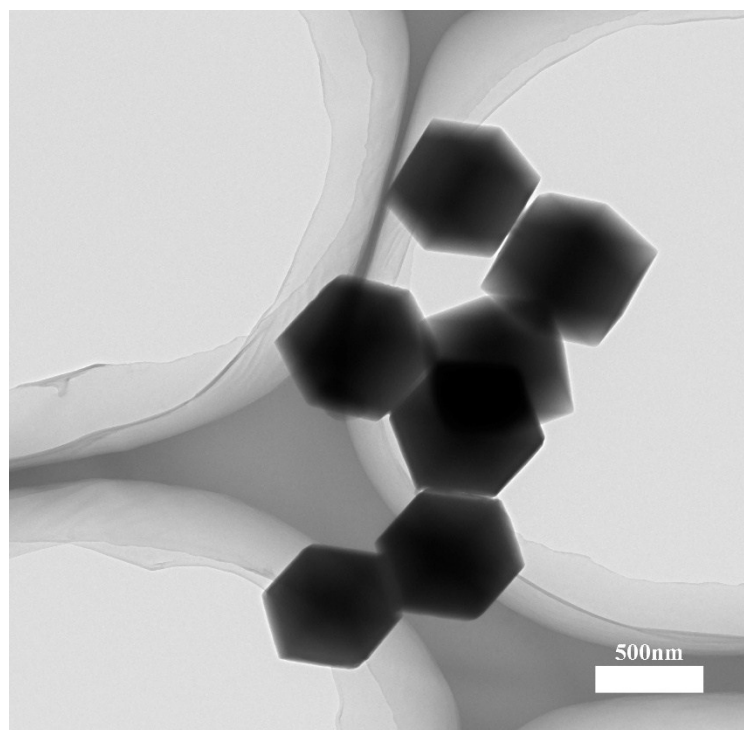


Fig. S8. TEM images of ZIF-67.

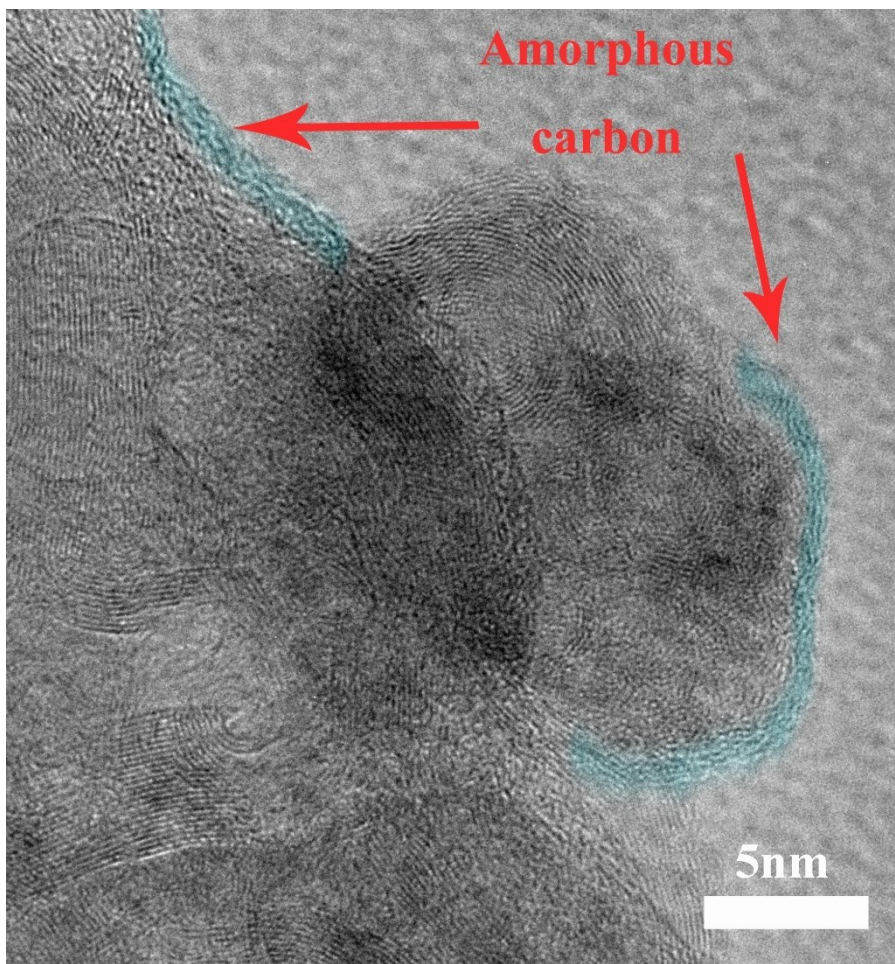


Fig. S9. HRTEM images of $\text{Co}_3\text{O}_4@\text{Z67-N700}@ \text{CeO}_2$.

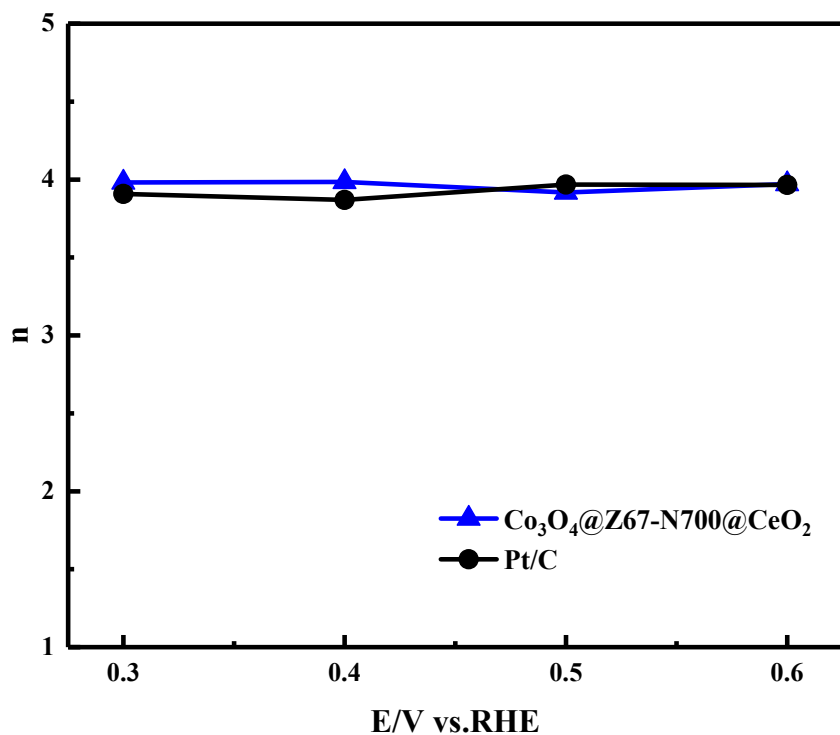


Fig. S10. Electron-transfer number n derived from K-L plots at different potentials.

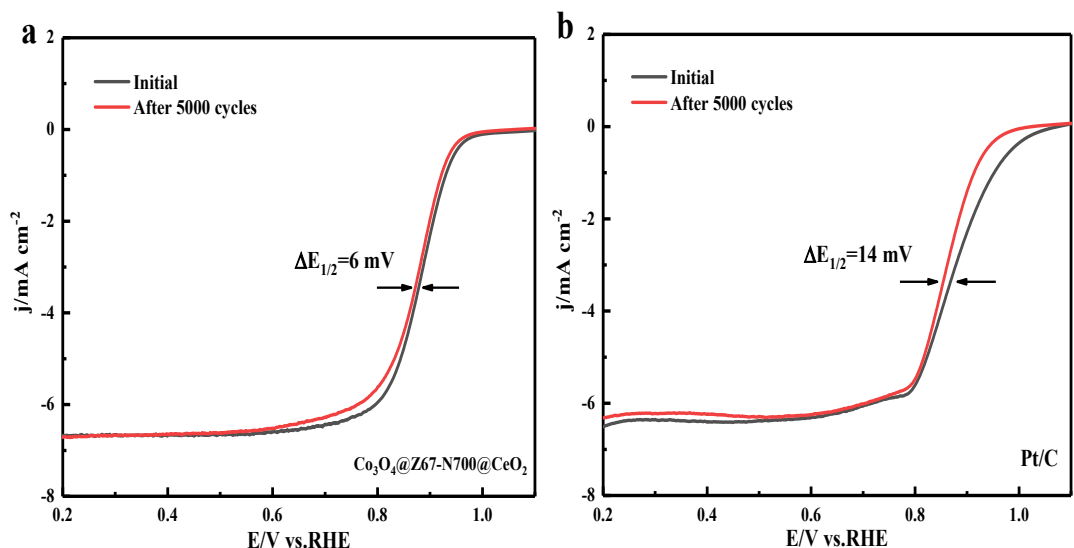


Fig. S11. ORR polarization curves of $\text{Co}_3\text{O}_4@\text{Z67-N700}@{\text{CeO}}_2$ (a) and Pt/C (b) before and after the continuous CV tests in the O_2 -saturated 0.1 M KOH at 1600 rpm.

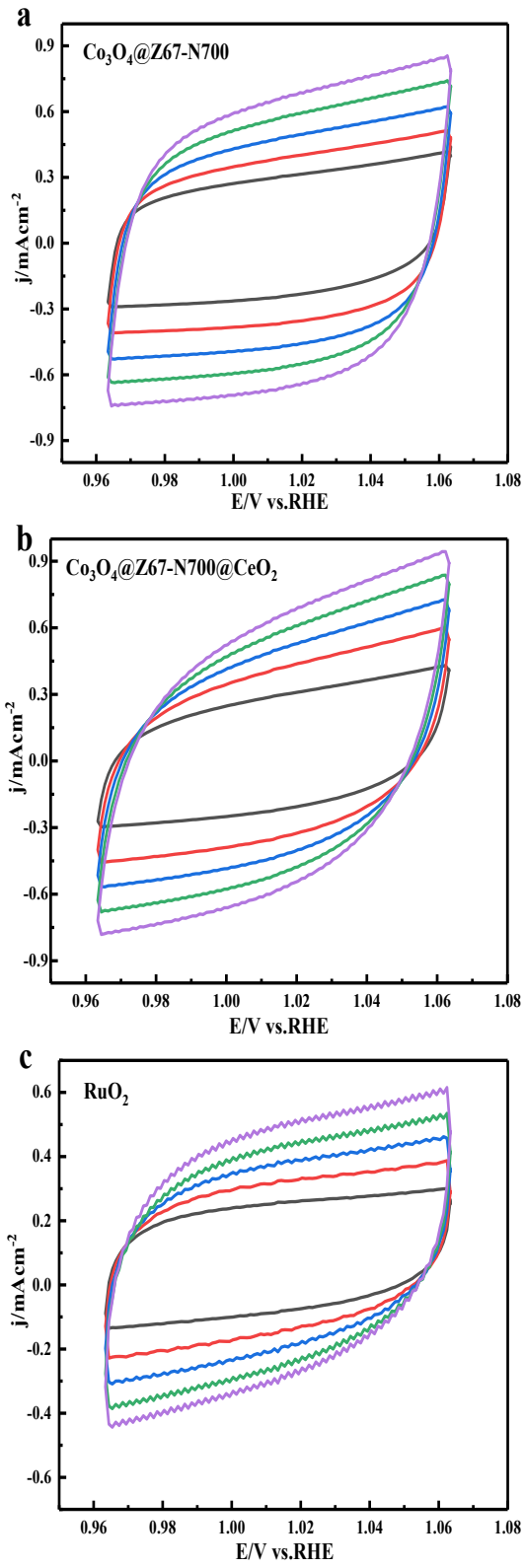


Fig. S12. Cyclic voltammograms with various scan rates from 40 to 120 mV s^{-1} of $\text{Co}_3\text{O}_4@\text{Z67-N700}$ (a), $\text{Co}_3\text{O}_4@\text{Z67-N700}@{\text{CeO}}_2$ (b), and RuO_2 (c).

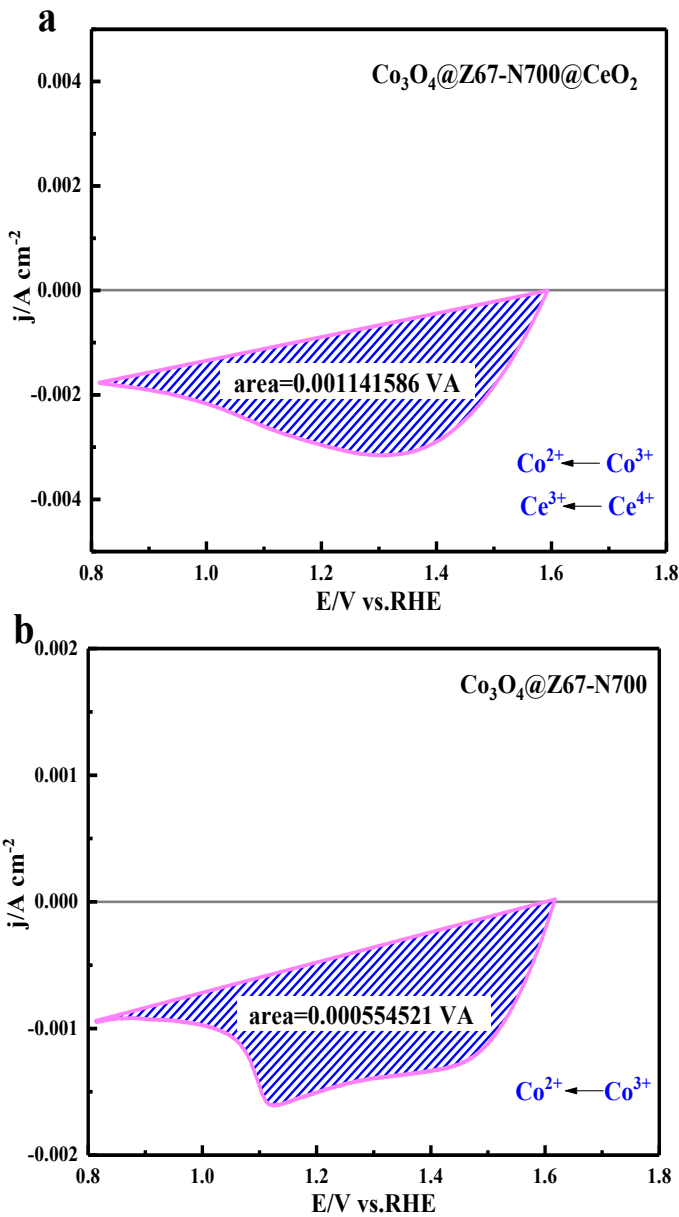


Fig. S13. CV of $\text{Co}_3\text{O}_4@\text{Z67-N700}@{\text{CeO}}_2$ (a) and $\text{Co}_3\text{O}_4@\text{Z67-N700}$ (b) showing the area of redox features considered for the calculation of number of surface active sites.

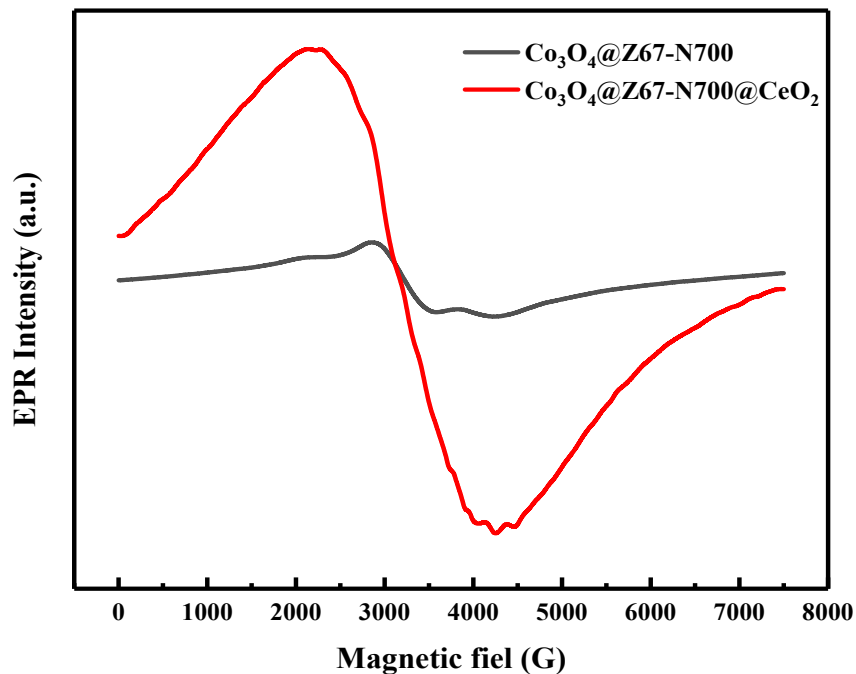


Fig. S14. The low temperature EPR spectra of the $\text{Co}_3\text{O}_4@\text{Z67-N700}$ and $\text{Co}_3\text{O}_4@\text{Z67-N700}@\text{CeO}_2$.

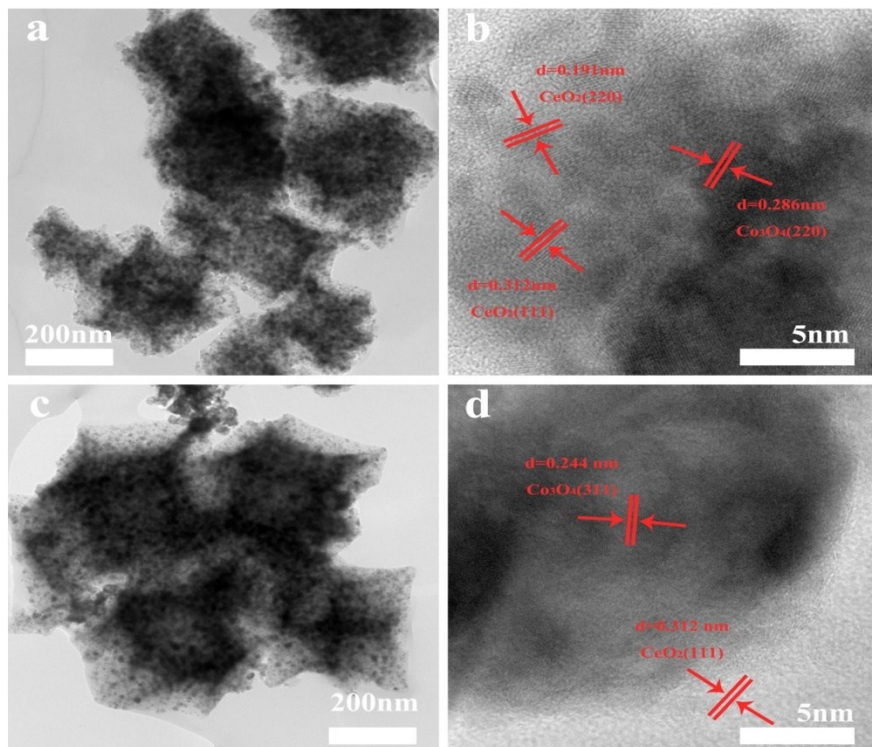


Fig. S15. TEM and HRTEM images for Co₃O₄@Z67-N700@CeO₂ after ORR (a and b) or OER (c and d) test.

References

- 1 S. Y. Pan, Z. Cai, Y. Q. Duan, L. Yang, B. Tang, B. J. Jing, Y. Dai, X. Xu and J. L. Zou, *Appl. Catal., B*, 2017, **219**, 18-29.
- 2 A. Sivanantham, P. Ganesan and S. Shanmugam, *Appl. Catal., B*, 2018, **237**, 1148-1159.
- 3 K. Karthick, S. Anantharaj, P. E. Karthik, B. Subramanian and S. Kundu, *Inorg. Chem.*, 2017, **56**, 6734-6745.
- 4 A. Sivanantham, P. Ganesan and S. Shanmugam, *Appl. Catal., B*, 2018, **237**, 1148-1159.
- 5 X. Shi, A. P. Wu, H. J. Yan, L. Zhang, C. G. Tian, L. Wang and H.G. Fu, *J. Mater. Chem. A*, 2018, **6**, 20100-20109.
- 6 K. Karthick, S. Anantharaj, P. E. Karthik, B. Subramanian, and S. Kundu, *Inorg. Chem.*, 2017, **56**, 6734-6745
- 7 S. L. Zhao, Y. Wang, J.C. Dong, C. T. He, H. J. Yin, P. F. An, K. Zhao, X. F. Zhang, C. Gao, L. J. Zhang, J. W. Lv, J. X. Wang, J. Q. Zhang, A. M. Khattak, N. A. Khan, Z. X. Wei, J. Zhang, S. Q. Liu, H. J. Zhao, and Z. Y. Tang, *Nat. Energy*, 2016, **1**, 16184.
- 8 J. D. Yang, J. X. Wang, L. Zhu, W. Zeng and J. F. Wang, *Mater. Lett.*, 2019, **234**, 331-334.
- 9 L. L. Chen, Y. Y. Li, N. Xu and G. A. Zhang, *Carbon*, 2018, **132**, 172-180.
- 10 W. Xia, R. Q. Zou, L. An, D. G. Xia and S. J. Guo, *Energy Environ. Sci.*, 2015, **8**, 568-576.
- 11 K. Liu, X. B. Huang, H. Y. Wang, F. Z. Li, Y. G. Tang, J. S. Li and M. H. Shao, *ACS Appl. Mater. Interfaces*, 2016, **8**, 34422-34430.
- 12 Y. S. Liu, H. B. Shen, H. Jiang, W. Z. Li, J. L, Y. M. Li and Y. Guo, *Int. J. Hydrogen Energy*, 2017, **42**, 12978-12988.
- 13 J. J. Chen, N. Zhou, H. Y. Wang, Z. G. Peng, H. Y. Li, Y. G. Tang and K. Liu, *Chem. Commun.*, 2015, **51**, 10123-10126.
- 14 X. Zhou, Y. J. Gao, S. W. Deng, S. Cheng, S. H. Zhang, H. Hu, G. L. Zhuang, X. Zhong and J. G. Wang, *Ind. Eng. Chem. Res.*, 2017, **56**, 11100-11110.
- 15 H. Zhou, D. P. He, A. I. Saana, J. L. Yang, Z. Wang, J. Zhang, Q. R. Liang, S. Yuan, J. W. Zhu and S. C. Mu, *Nanoscale*, 2018, **10**, 6147-6154.
- 16 Y. Y. Liang, Y. G. Li, H. L. Wang, J. G. Zhou, J. Wang, T. Regier and H. J. Dai, *Nat. Mater.*, 2011, **10**, 780-786.
- 17 M. Zhang, Y. L. Huang, J. W. Wang and T. B. Lu, *J. Mater. Chem. A*, 2016, **4**, 1819-1827.
- 18 R. C. Li, D. Zhou, J. X. Luo, W. M. Xu, J. W. Li, S. S. Li, P. P. Cheng and D. S. Yuan, *J. Power Sources*, 2017,

- 341**, 250-256.
- 19 S. W. Li, S. J. Peng, L. S. Huang, X. Q. Cui, A. M. Al-Enizi and G. F. Zheng, *ACS Appl. Mater. Interfaces*, 2016, **8**, 20534-9.
- 20 M. R. Gao, Y. F. Xu, J. Jiang, Y. R. Zheng and S. H. Yu, *J. Am. Chem. Soc.*, 2012, **134**, 2930-3.
- 21 Y. Hou, Z. H. Wen, S. M. Cui, S. Q. Ci, S. Mao and J. H. Chen, *Adv. Funct. Mater.*, 2015, **25**, 872-882.
- 22 J. H. Zhang, F. Li, W. B. Chen, C. S. Wang and D. D. Cai, *Electrochim. Acta*, 2019, **300**, 123-130.
- 23 D. J. Li, Z. G. Gu, W. H. Zhang, Y. Kang and J. Zhang, *J. Mater. Chem. A*, 2017, **5**, 20126-20130.
- 24 L. Q. Xu, X. Wang, L. L. Chai, T. T. Li, Yue. Hu, J. J. Qian and S. M. Huang, *Mater. Lett.*, 2019, **248**, 181-184.
- 25 B. Rezaei, A. R. T. Jahromi and A. A. Ensafi, *Int. J. Hydrogen Energy*, 2017, **42**, 16538-16546.
- 26 G. Xu, G. C. Xu, J. J. Ban, L. Zhang, H. Lin, C. L. Qi, Z. P. Sun and D. Z. Jia, *J. Colloid Interface Sci.*, 2018, **521**, 141-149.
- 27 T. J. Hu, Y. Wang, L. N. Zhang, T. Tang, H. Xiao, W. W. Chen, Man. Zhao, J. F. Jia and H. Y. Zhu, *Appl. Catal., B*, 2019, **243**, 175-182.
- 28 Z. Y. Guo, F. M. Wang, Y. Xia, J. L. Li, A. G. Tamirat, Y. R. Liu, L.Wang, Y. G. Wang and Y. Y. Xia, *J. Mater. Chem. A*, 2018, **6**, 1443-1453.
- 29 A. Sivanantham, P. Ganesan and S. Shanmugam, *Appl. Catal., B*, 2018, **237**, 1148-1159.
- 30 W. Ming. Zhang, X. Y. Yao, S. N. Zhou, X. W. Li, L. Li, Z. Yu and L. Gu, *Small*, 2018, **14**, 1800423-1800430.
- 31 J. J. Ban, G. C. Xu, L. Zhang, G. Xu, L. J. Yang, Z. P. Sun and D. Z. Jia, *Nanoscale*, 2018, **10**, 9077-9086.
- 32 Z. Z. Liang, C. C. Zhang, H. T. Yuan, W. Zhang, H. Q. Zheng and R. Cao, *Chem. Commun.*, 2018, **54**, 7519-7522.
- 33 A. Ajaz, J. Masa, C. Rosler, W. Xia, P. Weid, A. J. R. Botz, R. A. Fischer, W. Schuhmann and M. Muhle, *Angew. Chem., Int. Ed. Engl.*, 2016, **55**, 4087-4091.
- 34 Y. H. Tian, L. Xu, J. Bao, J. C. Qian, H. N. Su, H. M. Li, H. D. Gu, C. Yan and H. N. Li, *J. Energy Chem.*, 2019, **33**, 59-66.
- 35 M. Khalid, A. M. B. Honorato, H. Varela and L. M. Dai, *Nano Energy*, 2018, **45**, 127-135.
- 36 H. H. Ning, G. Q. Li, Y. Chen, K. K. Zhang, Z. Gong, R. F. Nie, W. Hu and Q. H. Xia, *ACS Appl. Mater. Interfaces*, 2019, **11**, 1957-1968.